# Full Optical Simulation of Partly Cloudy Scenes

Robert Sundberg[a,*], Steven Richtsmeier[a]

[a] Spectral Sciences, Inc., 4 Fourth Avenue, Burlington, MA 01803-3304, USA - (rob, s.richtsmeier)@spectral.com

**Abstract - This paper discusses recent advances in the full spectral simulation of scenes with partial cloud cover. We examine the effect of broken cloud fields on the solar illumination reaching the ground. Application of aerosol retrieval techniques in the vicinity of broken clouds leads to significant over-prediction of aerosol optical depth because of the enhancement of visible illumination due to scattering of photons from clouds into clear patches. These illumination enhancement effects are simulated for a variety of broken cloud fields using the MCScene code, a high fidelity model for full optical spectrum (UV through LWIR) spectral image simulation. MCScene provides an accurate, robust, and efficient means to generate spectral scenes for algorithm validation. MCScene utilizes a Direct Simulation Monte Carlo approach for modeling 3D atmospheric radiative transfer (RT), including full treatment of molecular absorption and Rayleigh scattering, aerosol absorption and scattering, and multiple scattering and adjacency effects.**

**Keywords:** Spectral, simulation, scene, algorithm, sensor, visible, infrared

## 1. INTRODUCTION

The effects of broken cloud fields on aerosol retrieval is an active area of research (Wen *et al.,* 2006; Marshak *et al.*, 2008). Application of aerosol retrieval techniques in the vicinity of broken clouds, even as far as several kilometers away, leads to significant over prediction of aerosol optical depth because of the enhancement of visible illumination from the scattering of photons from the clouds into clear patches. Several recent papers have examined the impact of 3D clouds on reflectance and aerosol optical depth retrieval (Wen *et al.,* 2006; Marshak *et al.*, 2008; Kassianov *et al.*, 2008, 2009). This paper presents detailed simulations of the enhanced solar illumination reaching the ground due to scattering from nearby cloud fields. The consequence of this enhanced illumination on aerosol retrieval will be presented in a future publication.

In this paper, we investigate the effect of broken cloud fields on solar illumination reaching the ground. The simulations presented here use a first-principles, high-fidelity spectral image simulation capability, dubbed MCScene, that is based on a Direct Simulation Monte Carlo (DSMC) approach for modeling the 3D radiative transport. The basic methodology used in MCScene has been described previously (Richtsmeier *et al.,* 2001, 2008; Sundberg *et al.,* 2005).

## 2. EFFECT OF FINITE 3D CLOUDS

To examine the illumination variations caused by clouds, a highly controlled scene was constructed with a cloud field containing 2 km by 2 km by 1 km (width, length, thickness) rectangular clouds that have a base altitude of 1 km and an optical depth of 10 above a terrain which has a uniform reflectance of 0.25. Figure 1 shows segment of the scene for a nadir view from 20 km which is approximately 9 km by 9 km. The sun is located to the west (left of the scene) with a solar zenith of 10 degrees. Concentrating on the central row of clouds, the observer "sees" under the cloud to the left which increase the area of the cloud shadow and some of the cloud edge is also observed, the cloud in the center of the image has a shadow which is partially blocked by the edge of the cloud and the cloud on the right also shows some edge effects. A horizontal slice across this image is compared to a scene without clouds for three spectral bands: 470, 665, and 870 nm in Figure 2. In this figure the percent difference between the cloudy and no cloud scene is plotted. There is a significant variation in the shadow depths and the amount of scattered radiation in the cloud free areas of the scene with spectral channel. The darkest shadows are produced at the longer wavelengths which have a slightly lower scattering albedo and a smaller forward scattering lobe than the blue light. These two effects tend to reduce the number of longer wavelength photons which reach the ground in the shadowed area and increases the number of photons which reach the sunlit area causing an enhancement on the order of 20%. The blue photons have a near unity scattering albedo and a larger forward scattering peak in their phase function which tends to brighten the shadowed region and cause a smaller illumination enhancement to the sunlit regions.

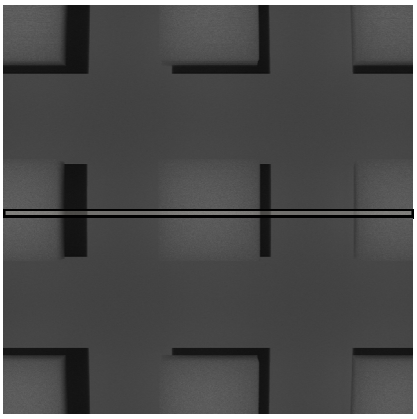

Figure 1. MCScene single band image for rectangular synthetic cloud field. The region shown in Figure 2 is highlighted.

* Corresponding Author

** The authors wish to acknowledge Spectral Sciences, Inc. for support under an internal research and development grant, and the Air Force Research Laboratory, RVBYM for support under contract number FA8718-07-C-0048.

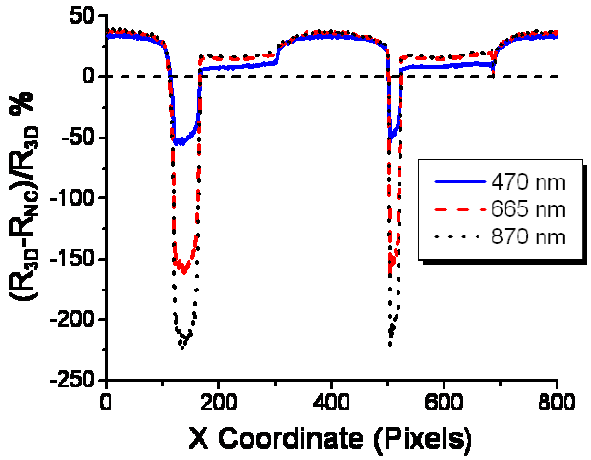


Figure 2. Percent enhancement of top-of-the-atmosphere apparent reflectance for slice across rectangular cloud field shown in Figure 6 for three spectral channels.

While Figure 1 depicts a simple scattering scenario, complicated cloud fields yield more complicated secondary illumination effects. Simulations with realistic cloud fields and the resulting enhancement results are shown in Figures 3-6. Three synthetic cloud fields for the simulations were generated by the Cloud Scene Simulation Model (CSSM) (Cianciolo and Raffensberger, 1996) CSSM generates high fidelity cloud liquid water content fields in four dimensions based on fractal techniques and using meteorological inputs. The spatially varying optical depths (OD) of the cloud fields generated for this study are shown in Figure 3. The nimbostratus field has a maximum optical depth of 24, while the altostratus and stratocumulus street fields have OD maxima of 9 and 21, respectively. Figure 4 shows a series of images simulated using the three cloud types over flat terrain with a spectrally uniform reflectance of 0.10. For all cases, the sensor was nadir-viewing from 20 km altitude. The MODTRAN® (Berk *et al.,* 1989, 2006) atmosphere for these simulations was the mid-latitude summer model with rural aerosols and 23 km ground visibility. Local time for the simulation of Figure 4A was solar noon (i.e., sun from due south) with a solar zenith angle of 17.4º. For the altostratus scene in Figure 4B, local time was solar noon minus 2 hours with a solar zenith angle of 30.5º. Local time for Figure 4C was solar noon plus 2 hours with a solar zenith angle of 30.5º.

The percent change in scene apparent reflectance at 660 nm when compared to the cloud free scene is shown in Figure 5 for each of the three cloud fields. The three scenes represent different scattering scenarios. In Figure 5A, a high south sun shines on a thick nimbostratus field, and photons are backscattered off the clouds onto the open ground to the south. There is little shadowing apparent as the shadows fall underneath the cloud field. Almost all open areas in the scene exhibit enhanced brightness ranging from about 30% near the clouds down to 5% at the bottom edge of the scene, several km away from the cloud field. There are also areas visible through holes in the clouds where the enhancement runs from 30% to as high as 64%. Here, the holes or convoluted cloud field edges serve as conduits for photons.

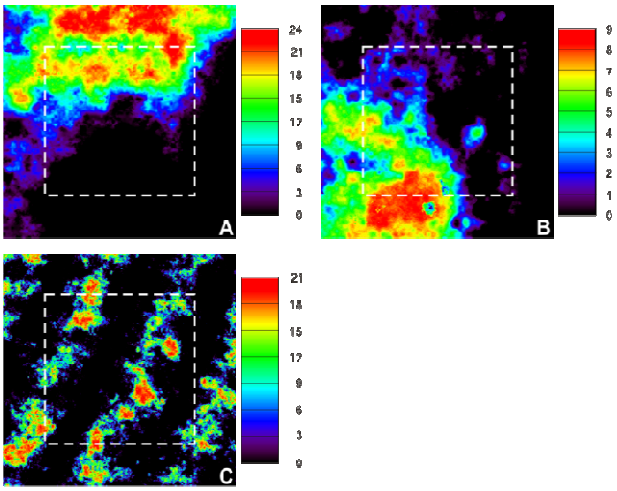


Figure 3. Vertical optical depth maps for three types of cloud fields: (A) nimbostratus, (B) altostratus, and (C) stratocumulus street. The cloud fields measure 15 km on a side. The dashed squares indicate the fields-of-view for the simulations.

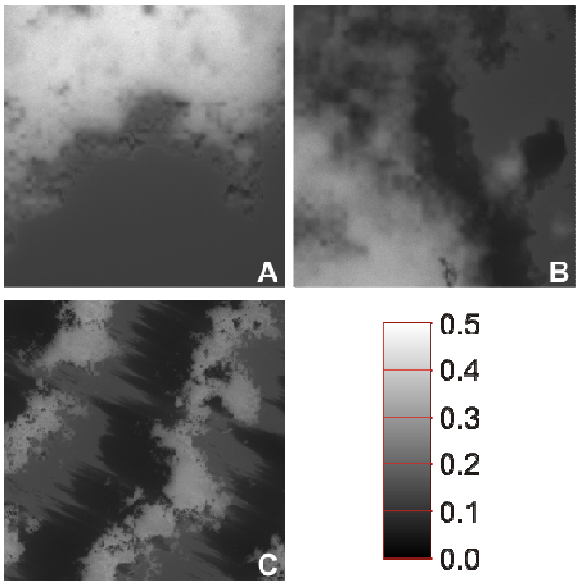


Figure 4. Apparent reflectance for a sensor band of 660±5 nm for scenes containing three types of cloud fields: (A) nimbostratus, (B) altostratus, (C) stratocumulus street, over flat terrain with uniform reflectance of 0.10. Sensor fields-of-view are 10 km x 10 km.

In Figure 5B, the sun comes from the south west at 30.5º over the top of a moderately dense altostratus field. There are shadows of varying depth due to the spatially varying density of the cloud field. There is significant enhancement apparent in unshaded areas, ranging from about 15% near shadow edges down to about 3% at the furthest distance from the clouds. Whereas the enhancement in the nimbostratus scene was due to backscattering, the enhancement in Figure 5B is due predominately to forward scattering of photons off of or through the cloud tops.

Figure 5C effectively represents a mix of the scenarios of 5A and 5B, as a 30.5º sun shines from the south west, perpendicular to the roughly parallel rows of a stratocumulus street field. Here, backscattering from the eastern face of a cloud row is met by the forward scattering and shadows from its eastern neighbor row. As a result, enhancement is noticeably greater in unshaded areas than for either of the nimbostratus or altostratus scenarios. As was the case for the nimbostratus scene, convoluted cloud edges facing the sun result in greater enhancement near the clouds. The shadows in the stratocumulus scene are more dense than the altostratus shadows (as the clouds are more dense), but the edges of these shadows are softened by the backwash of photons from a neighboring row of clouds.

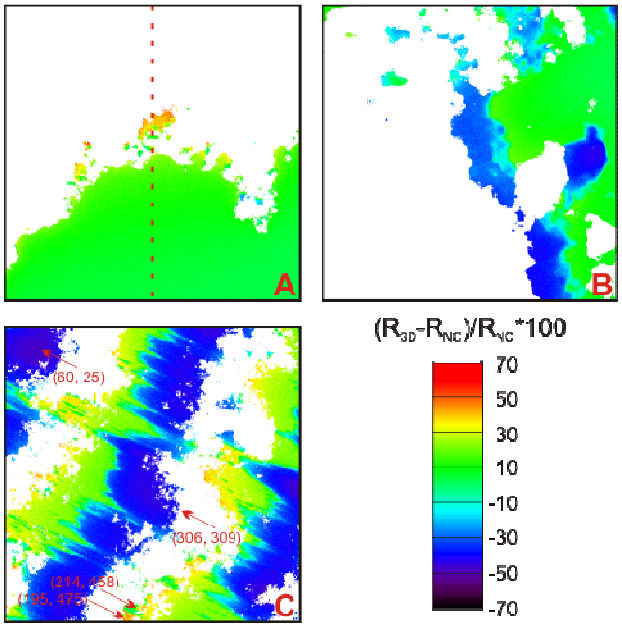


Figure 5. Percent enhancement to apparent reflectance for 660±5 nm for scenes with three synthetic cloud fields: (A) nimbostratus, (B) altostratus, and (C) stratocumulus street. Pixels containing cloud are masked white. The red dashed line in "A" marks the path of the enhancement profile of Figure 6. Reflectance spectra for labeled pixels in C are plotted in Figure 7.

Reflectance spectra for several pixels labeled in Figure 5C are shown in Figure 6. These include a cloud top pixel, a pixel in deep shadow, one exhibiting near-maximum enhancement for this scene, and one that mixes enhancement and shadow. Also shown for reference is a cloud-free spectrum and the uniform source reflectance for the ground. There is a spectral dependence to the enhancement effect. Comparing the "enhanced" and "no cloud" pixels, enhancement is greater in the infrared than the visible, approaching a factor of two from 800 to 1800 nm. Comparing the "shadow" and "no cloud" curves, shadows are deeper in the infrared, presumably because they are not back-filled by Rayleigh scattering as they are in the visible. Curiously, comparing the mixed "enhanced + shadow" curve with the "no cloud" curve shows that they are nearly identical from about 1100 nm to longer wavelengths.

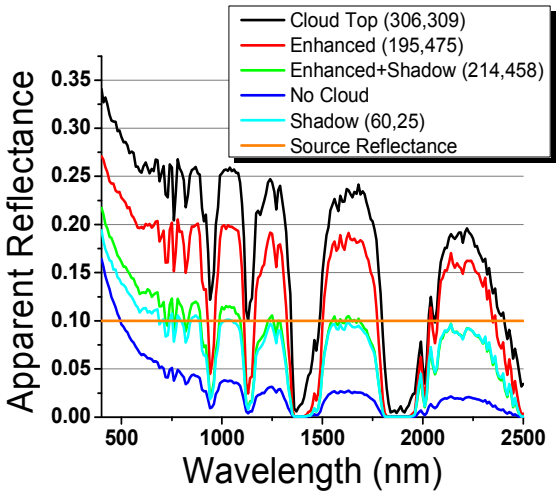


Figure 6. Comparison of pixel spectra for several points from Figure 5C, along with the spectrum from a cloudless scene, and a line marking source reflectance of the ground.

We have recently been developing an additional feature allowing for simulations for an up-looking sensor. Some preliminary results are presented in Figure 7. For these simulations, the observer is placed on the ground and looks up with a full hemispherical view of the sky. At left, the observer sees the altostratus cloud field of Figure 4 with the local time set to solar noon plus two hours. At right, the observer sees the stratocumulus street field with the local time set to solar noon minus two hours. In both cases, the observer stands in shadow at the centers of the respective scenes of Figure 4. In the altostratus image, the cloud bottom appears brightest where the solar position is roughly aligned with a thin spot in the clouds (position "1"). In the stratocumulus image, where the sun comes from the lower right, the brightest illumination comes from where the photons skim the top of the eastern "street". Representative spectra from the positions marked in the altostratus scene are shown in Figure 8.

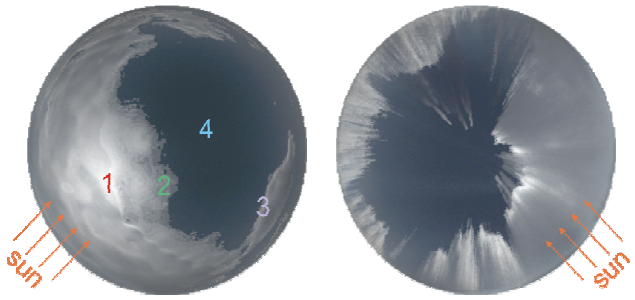


Figure 7. RGB composite hemispherical images, from the ground looking up, from the centers of the altostratus (left) and stratocumulus street (right) scenarios of Figure 4.

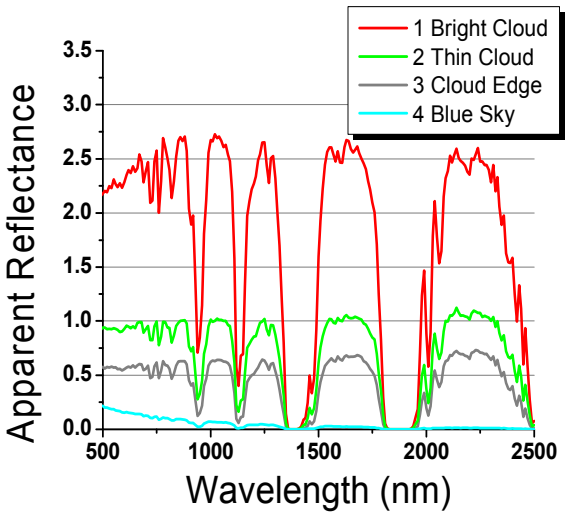


Figure 8. Representative spectra from the look-up image for the altostratus scene of Figure 9.

## 3. CONCLUSIONS

A practical, first-principles simulation model for spectral imagery, based on a Direct Simulation Monte Carlo (DSMC) radiative transport approach, has been used to investigate the enhanced radiation in sunlit areas caused by scattering of photons from broken cloud fields. The enhancement shows spectral and spatial dependence and is present in both forward and back scattering scenarios. The effect diminishes as distance from the cloud increases. Key parameters to developing a model for the effect include cloud type and density, and the coupling of solar position with cloud spatial geometry. In the visible part of the spectrum, deep clouds shadows have more blue photons because these photons are scattered better, have a higher single scattering albedo, than green or red photons. The enhancement also shows a spatial dependence with greater enhancement being closer to the cloud and the enhancement falls off away from the clouds, but for all cases examined there is still significant enhancement several kilometers away from the cloud field. In the optically thick nimbostratus simulation, there is a 5% enhancement 5 km away from the cloud field (far lower right of scene in Figure 5A).

In a future paper the effects of broken cloud fields on aerosol retrieval will be examined. Application of aerosol retrieval techniques in the vicinity of broken clouds leads to significant over prediction of aerosol optical depth because of the enhancement of visible illumination from the scattering of photons from the clouds into the clear patches. Simulations such as shown in this paper should help in developing a technique to produce accurate aerosol optical depths near broken clouds.

## REFERENCES

A. Berk, L.S. Bernstein, and D.C. Robertson, "MODTRAN®: A Moderate Resolution Model for LOWTRAN 7," GL-TR-89-0122, Geophysics Directorate, Phillips Laboratory, Hanscom AFB, MA 01731 ADA214337 (April 1989).

A. Berk, *et al*., "MODTRAN®5: 2006 update," In Algorithms for Multispectral, Hyperspectral, and Ultraspectral Imagery XII, Sylvia S. Chen, Paul E. Lewis, Editors, Proceedings of SPIE Vol. 6233, (2006).

M.E. Cianciolo, and M.E. Raffensberger, "Atmospheric Scene Simulation Modeling and Visualization (AMV)," Cloud Scene Simulation Model User's Guide, TIM-07169-2, TASC, Reading, MA, (1996).

E. Kassianov, M. Ovtchinnikov, "On reflectance ratios and aerosol optical depth retrieval in the presence of cumulus clouds," Geophys. Res. Lett. 35: L06807 (2008).

E. Kassianov, M. Ovtchinnikov, L. Berg, S. McFarlane, and C. Flynn, "Retrieval of aerosol optical depth in vicinity of broken clouds from reflectance ratios: Sensitivity study," JQSRT doi:10.1016/j.jqsrt.2009.01.014 (2009).

A. Marshak, G. Wen, J. Coakly, L. Remer, N. Loeb, R. Cahalan, "A simple model for the cloud adjacency effect and the apparent bluing of aerosols near clouds," J. Geophys. Res. 113:D14S17 (2008).

S.C. Richtsmeier, A. Berk, S.M. Adler-Golden, and L.S. Bernstein, "A 3D Radiative-Transfer Hyperspectral Image Simulator for Algorithm Validation," Proceedings of ISSSR 2001, Quebec City, Canada (June 2001).

S. Richtsmeier, R. Sundberg, and F.O. Clark, "Fast Monte Carlo Full Spectrum Scene Simulation," Proceedings of the International Radiation Symposium 2008, Foz do Iguaçu, Brazil (August 2008).

R.L. Sundberg, R. Kennett, S.C. Richtsmeier, J. Gruninger, A. Berk, and M. Matthew, "Hyperspectral Scene Simulation in the Ultraviolet through Longwave Infrared," Phase II Final Report, prepared for AFRL, Sensors Directorate WPAFB, under Contract No. F33615-02-C-1167 (2005).

G. Wen, A. Marshak, R. Cahalan, "Impact of 3D clouds on clear sky reflectance and aerosol retrieval in a biomass burning region of Brazil," J. Geophys. Res. 112:.D13204 (2006).